Programmable Mechanical Properties of Two-Photon Polymerized Materials: From Nanowires to Bulk

Jens Bauer, Anna Guell Izard, Yunfei Zhang, Tommaso Baldacchini, and Lorenzo Valdevit*

Two-photon polymerization direct laser writing (TPP-DLW) is the most promising technology for additive manufacturing of geometrically complex parts with nanoscale features, and could dramatically accelerate the development of a wide range of engineering micro/nanosystems. However, a major obstacle to TPP-DLW's widespread industrial adoption is the lack of systematic data on material properties and limited knowledge on their correlation with processing parameters. These correlations for the acrylate-based resin IP-Dip are experimentally established over a large range of process parameters and length scales ranging from nanometers to centimeters. Universal characteristic relations between mechanical properties and process parameters are identified, which enable the tailoring of the material strength and stiffness over half an order of magnitude from rubbery soft to hard and strong. With a threshold-based optics model presented herein, the mechanical properties of the two-photon polymerized material can be accurately captured as a function of the applied process parameters, laying the foundation for a universal quantitative predictability of two-photon polymerization with programmable mechanical properties. This knowledge enables fabrication of microscale components with tailored local gradients in their mechanical properties, with significant implications for the development of novel mechanical, photonic, and photonic metamaterials.

1. Introduction

Additive manufacturing is rapidly advancing toward widespread industrial usability, with two-photon polymerization

direct laser writing (TPP-DLW) being the most versatile technology for fabricating 3D meso, micro, and nanoscale parts.[1–3] Some of the most prominent research fields accelerated by TPP are photonic and mechanical metamaterials,[4–6] microactuators,[7,8] microrobots,[9–11] bioscience,[12–14] and biomimetics.[15–17] Microfluidic and biomedical devices,[18–22] microoptical elements on fiber-tips,[23–25] and chip-to-chip interconnects,[26,27] may soon become the first industrial applications.

While TPP technology is rapidly progressing,[3] fabrication is still largely empirical, hindered by the lack of systematic data on material properties (e.g., strength and stiffness), and limited knowledge on their dependence on the process parameters. A small number of studies have reported certain properties of two-photon polymerized materials.[28–32] However, most studies were specific to particular, application-relevant specimen geometries and sizes, with limited general implication on the establishment of TPP processing-structure–properties relations. Mechanical properties like strength and stiffness have not been studied, or were estimated from indirect measurements, respectively.[29–31] By contrast, for additive manufacturing processes which have experienced wide-spread industrial adoption (e.g., fused deposition modeling and direct metal laser sintering), processing–microstructure–properties relationships have been studied extensively,[33–36] with the overarching goal of understanding all the underlying physical mechanisms. Clearly, TPP will not reach significant industrial penetration until precise and reliable specification and control of material properties are established.

TPP uses a focused ultrafast pulsed laser beam to locally expose a photosensitive material by two- or multi-photon absorption.[1] Polymerization only occurs within a confined ellipsoid-shaped volume in the focal point of the laser beam. This volume element, or voxel, is the most elemental TPP feature. Smallest reported voxels dimensions are below 100 nm,[1,3] while typical widths and heights are ≥200 nm and ≥600 nm, respectively. TPP-derived parts are generally hatched from multiple voxel-lines, i.e., continua of voxels, in a line-by-line fashion, using galvanometric mirrors and 3-axis stages.

Dr. J. Bauer, A. Guell Izard, Prof. L. Valdevit
Mechanical and Aerospace Engineering Department
University of California
Irvine, CA 92697, USA
E-mail: valdevit@uci.edu
Y. Zhang, Prof. L. Valdevit
Materials Science and Engineering Department
University of California
Irvine, CA 92697, USA
Dr. T. Baldacchini
Schmid College of Science and Technology
Chapman University
One University Drive
Orange, CA 92866, USA

The most common TPP materials are negative-tone acrylate-based resins,[37,38] due to their processing ease and the wide assortment of functionalities and monomer sizes.[39] Other successfully employed materials include epoxies, most notably SU-8,[40] hydrogels,[41] organic–inorganic hybrids,[42] proteins,[43] and elastomers like PDMS.[44] In the simplest case, acrylate resins consist of a monomer, which will be cross-linked, and a photoinitiator, which absorbs light and cleaves into free radicals which then start the polymerization reaction. During polymerization via radical chain growth, several initiation, propagation, and termination reactions, each with their own different rates, occur simultaneously. Monomers react only with the propagating reactive center, not with other monomers, and chain addition ceases when the concentration of radicals is depleted by a number of termination reactions. Although reaction kinetics differ,[45] the fundamental mechanisms which impact mechanical properties are often similar,[46,47] and comparable dependencies on TPP process parameters may be expected.

The mechanical properties of acrylate-based resins are related to the degree of conversion (DC), i.e., the extent of cross-linking between polymer chains, which itself correlates with the exposure dose of light (D) during fabrication. The DC can be assumed proportional to the number of radicals generated within a volume element.[48] Neglecting diffusion mechanisms,[49] the density of radicals (ρ) is given by the two-photon absorption rate equation

$$\frac{d\rho}{dt} = (\rho_0 - \rho)\,\delta_{2,\mathrm{eff}} I^2 \tag{1}$$

with the photoinitiator concentration in the uncured photoresist (ρ_0), the effective two-photon cross section ($\delta_{2,\mathrm{eff}}$) and the spatial photon flux intensity distribution (I), corresponding to the typically Gaussian spatial laser beam profile at the focal point.[46] Integration of Equation (1) gives the dependency of ρ on D as

$$\rho = \rho_0 \left(1 - e^{-\delta_{2,\mathrm{eff}} D}\right) \tag{2}$$

where D is the integral of I^2 over the exposure time (t). The solubility of negative-tone photoresists is a highly nonlinear function of the exposure dose, causing a distinct threshold behavior, whereby a polymerized photoresist network remains soluble below a threshold exposure dose (D_{th}). This means that sustainable polymerization able to withstand a solvent bath requires $D \geq D_{\mathrm{th}}$. Conversely, above a certain damage threshold, the photoresist may boil. The ratio of damage to polymerization threshold is the dynamic range of the photoresist. Equivalent relations are valid for cationic polymerization of epoxies.[47]

Three key TPP process parameters determining the exposure dose, as well as the fabrication duration and accuracy, are the laser average power (P), the writing speed (v), and the writing density, which can be quantified by the hatching distance (d_{h}) and the slicing distance (d_{s}) between neighboring voxel-lines.[50] Based on the TPP model discussed above, D can be expressed as

$$D = D_{\mathrm{o}}\, D_{\mathrm{V}} \propto \frac{P^2}{v} D_{\mathrm{V}} \tag{3}$$

with the spatial exposure dose distribution (D_{V}), relative to the peak value (D_{o}).[47,51] D_{o} can be expressed in terms of P, v, and D_{V} correlates with the spatial intensity profile of the laser beam. For a hatched material, D_{V} is a function of d_{h} and d_{s}.

Development of meaningful and reliable mechanical property data of two-photon polymerized materials requires the systematic characterization across the entire dynamic range, on all relevant length-scales. The size of a solitary voxel-line feature and its mechanical properties correspond to the above-threshold portion of the Gaussian intensity profile of the laser beam. Surrounding polymerized material corresponding to the below-threshold wings of the profile is dissolved during development. When several voxel-lines are printed with the same process parameters in sufficient proximity, the doses of the sequential exposures accumulate, with the photoresist "remembering" previous below- and above-threshold exposures. Depending on the applied process parameters, this "memory effect" may further cross-link already insoluble material, or form new, less cross-linked material by the overlap of below-threshold Gaussian wings.[52] Enclosed minima may permanently remain below threshold, resulting in weak regions within a polymerized part. In practice, this ideal memory effect is superimposed to time-dependent processes, such as molecular diffusion.[45] Thus, the effective properties of TPP-derived parts are a nontrivial function of the properties of the corresponding constituent features.

In this paper, we systematically characterize the mechanical properties of the two-photon polymerized acrylate-based resin IP-Dip. We report the direct measurement of the mechanical properties of individual voxel-line features and derive the mechanisms controlling the effective mechanical properties of TPP-derived hatched parts. Specimens spanned multiple length-scales, from 190 nm to centimeters (**Figure 1**a), including nanowires consisting of individual voxel-lines, multi-voxel-line bars and conventionally cured bulk samples. We measure Young's modulus (E), yield strength (σ_{y}), ultimate tensile strength (σ_{UTS}), and degree of conversion by uniaxial compression and tension experiments and Raman microspectroscopy, respectively (Figure 1b–d). We find that the mechanical properties of solitary voxel-lines are largely independent on their size and the applied TPP process parameters, suggesting the existence of a mobility threshold which counterbalances the expected process parameter-sensitivity. In contrast, multi-voxel-line hatched parts can be vastly tailored from rubbery soft to hard and strong, depending on the degree of "overlap" of constituent voxel-line features. We identify universal characteristic trends for the mechanical properties, which hold over a large range of process parameter combinations. We quantify the observed behavior with a threshold-based optical model, which accurately captures the mechanical properties of the two-photon polymerized material as a function of the applied process parameters. This study provides a database to systematically tailor process parameters depending on the required mechanical properties, precision and process time for IP-Dip and lays the foundation for a universal quantitative predictability of the mechanical properties of TPP-derived parts. While IP-Dip is one of the most commonly used TPP materials, the fundamental physics unveiled in this work will apply to a wide range of photosensitive material systems.
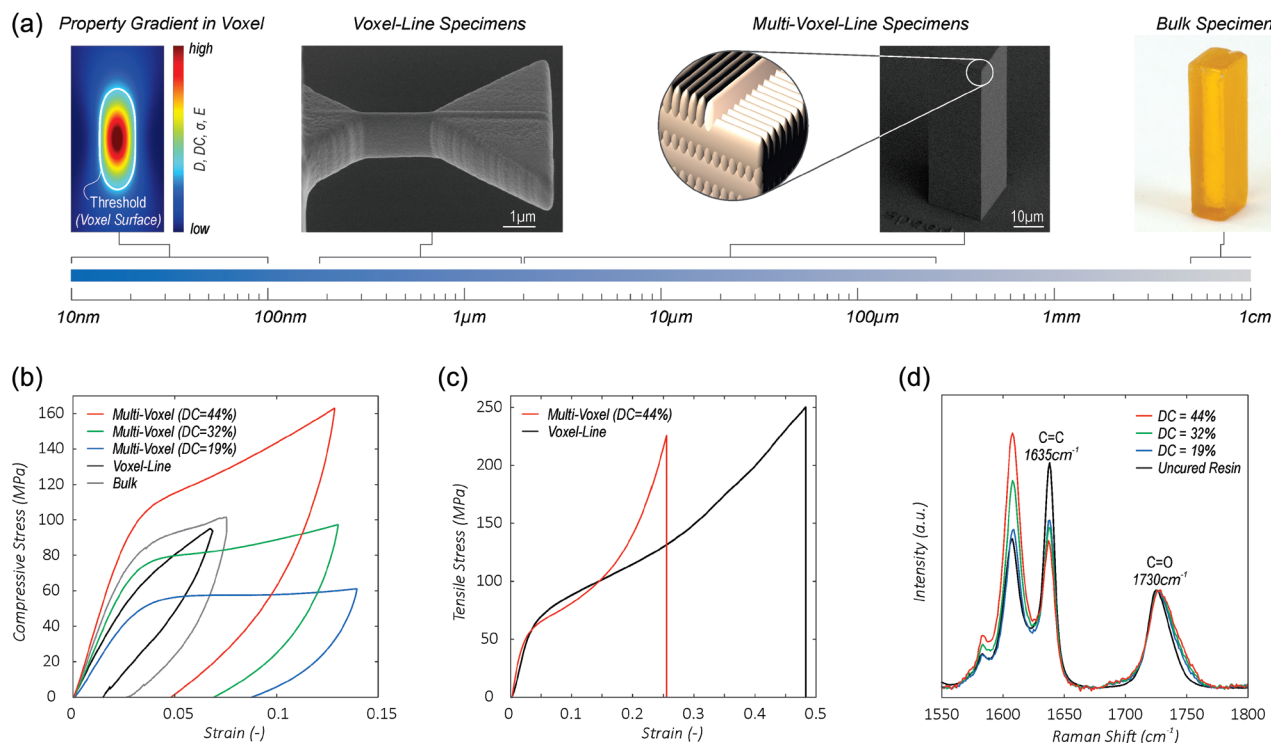
Figure 1. Mechanical characterization of the triacrylate TPP resin IP-Dip from nanowires to bulk, from polymerization to damage threshold. a) The investigated length scale ranges from sub-voxel gradients over individual voxel-lines and multi-voxel-line hatched specimens to conventionally cured bulk material. Representative b) compressive and c) tensile stress–strain curves and d) Raman spectra show the large tailorability of strength, stiffness and degree of conversion (DC) of multi-voxel-line hatched specimens compared to solitary voxel-lines and bulk specimens.

2. Results

2.1. Single Voxel-Line Specimens

Two-photon polymerized nanowire specimens are designed as dumbbell-shaped cantilever bars with one voxel-line in the gauge section, allowing for the direct measurement of the material strength and stiffness at the most elemental TPP level. Single voxel-line cantilevers are printed onto previously formed support blocks, and dumbbell sections are subsequently added by alternatingly printing additional lines on both sides. This symmetric printing strategy with sufficiently low writing speeds overcomes the typical warping of unsupported slender TPP features due to close-by exposures, resulting in high-quality specimens over the entire dynamic range of the photoresist. Customized support blocks provide easy accessibility without the need of additional specimen preparation. Figure 1b,c includes compressive and tensile stress–strain curves of specimens with ≈400 nm wide voxel-lines (Movies S1 and S2, Supporting Information). We find elasto-plastic behavior, with almost identical yield strength and stiffness under compression and tension. The material is remarkably tough, considering the high ultimate tensile strength of 255 ± 7 MPa with failure strains over 40%.

The mechanical properties of voxel-lines are found to be largely insensitive to their size and applied TPP process parameters (**Figure 2**). We manufacture 190–640 nm wide compression specimens, by varying the combination of laser average power and writing speed (Figure 2a). For a first set of specimens, we keep v constant at 10 µm s^{-1} and vary P across the entire dynamic range of the photoresist, with the smallest and the largest specimens at the polymerization and the damage threshold, respectively. A second set of specimens is manufactured with v spanning four orders of magnitude from 100 to 10 000 µm s^{-1}, where P was adjusted to yield ≈300 nm wide voxel-lines. Figure 2b shows the mechanical properties of both specimen sets as a function of the voxel-line size, while Figure 2c shows the mechanical properties as a function of P for specimens printed with v = 10 µm s^{-1}. Toward the polymerization threshold our data indicate a certain decrease in the Young's Moduli as well as to some extent in the compressive yield strengths. However, both E and σ_y plateau in a narrow range with average values of 48 ± 6 MPa and 2.4 ± 0.3 GPa, respectively.

2.2. Hatched Multi-Voxel-Line Specimens

In contrast to individual voxel-lines, the mechanical properties of hatched multi-voxel-line specimens show a pronounced dependency on the TPP process parameters (**Figure 3**), consistent with previously reported data.[28,31] We examine the impact of different combinations of laser average power, writing speed and writing density. E, σ_y, and DC are measured by uniaxial compression and by Raman spectroscopy of bars with nominal dimensions of $20 \times 20 \times 65$ µm, with a constant hatching-to-slicing-distance ratio ($d_s/d_h = 2$).

**ADVANCED
SCIENCE NEWS**
www.advancedsciencenews.com

**ADVANCED
MATERIALS
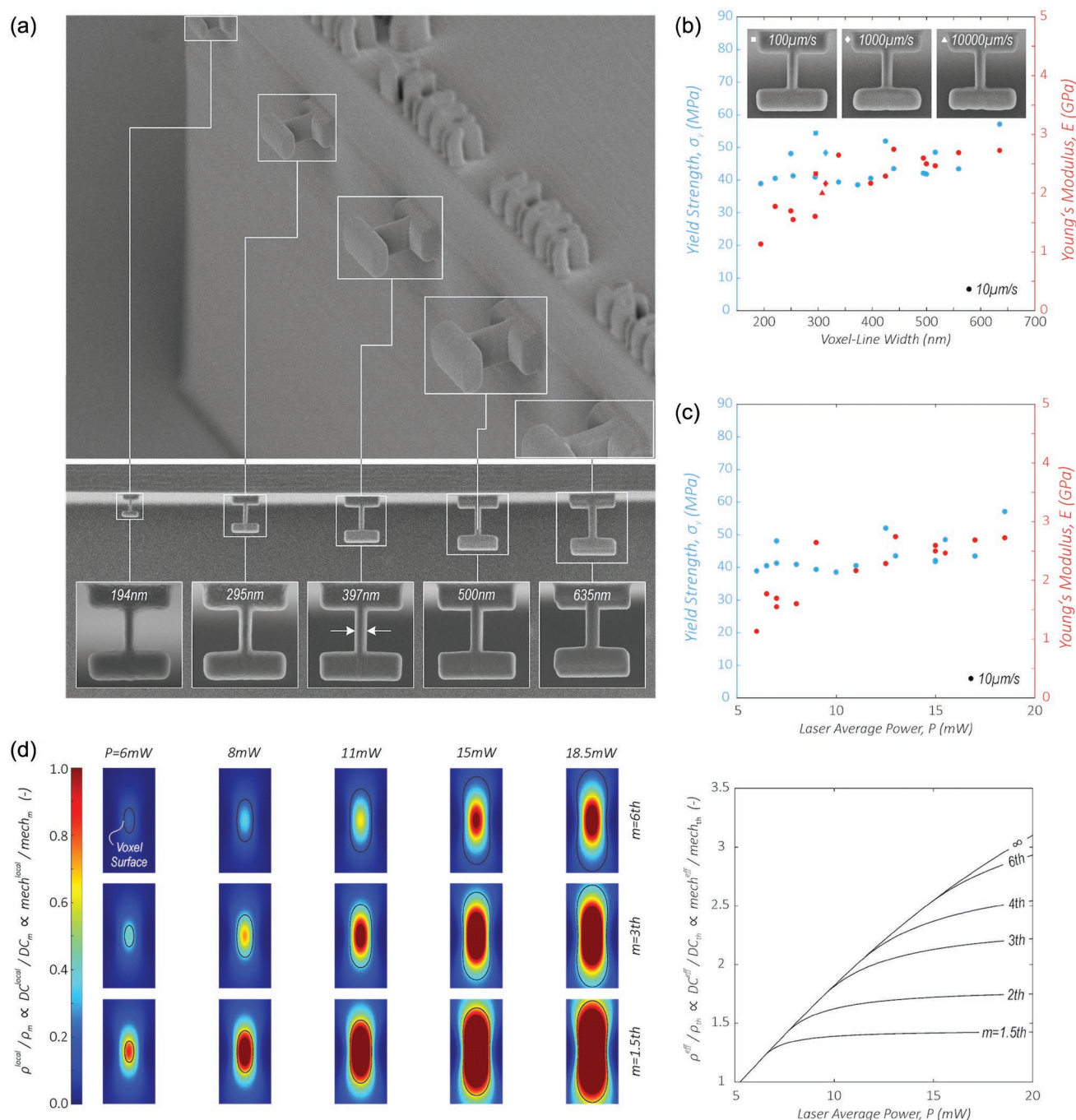TECHNOLOGIES**
www.advmattechnol.de

Figure 2. Mechanical properties of voxel-line features are found size and TPP process parameters independent. a) Varying the combination of laser average power (*P*) and writing speed (*v*) across the dynamic range of IP-Dip manufactures compression specimens with 195–660 nm wide voxel-lines. Compressive yield strength and Young's modulus versus b) voxel-line size and c) *P* (only specimens with *v* = 10 µm s⁻¹). d) Simulated radical density (*ρ*) in voxel-line cross-section depending on *P* (*v* = 10 µm s⁻¹); local gradients (left) and corresponding effective properties (right) considering a mobility threshold (*m*) which limits *ρ*, compated to a mobility threshold free material (*m* = ∞). Increasing (*m*) with respect to the polymerization threshold (th) reduces process-parameter sensitivity of *ρ*, degree of conversion (DC) and mechanical properties (mech).

P, *v*, and d_h each show a characteristic impact on the mechanical properties, allowing to tune *E* and σ_y across half an order of magnitude, from 0.6 to 3.6 GPa and from 20 to 70 MPa, respectively (Figure 3a). E, σ_y and DC increase with *P* and decrease with *v* and d_h. In all cases, specimens start to fully form with a DC above ≈20%; by comparison, the

damage threshold is just below ≈45% (Figure 3b). Decreasing mechanical properties are thereby accompanied by increasing shrinkage with respect to the nominal dimensions (Figure 3c and Figure S1, Supporting Information). Correlating with emerging porosity for $d_h \geq 0.45$ µm, the DC plateaus above ≈20%, whereas the mechanical properties drop. For
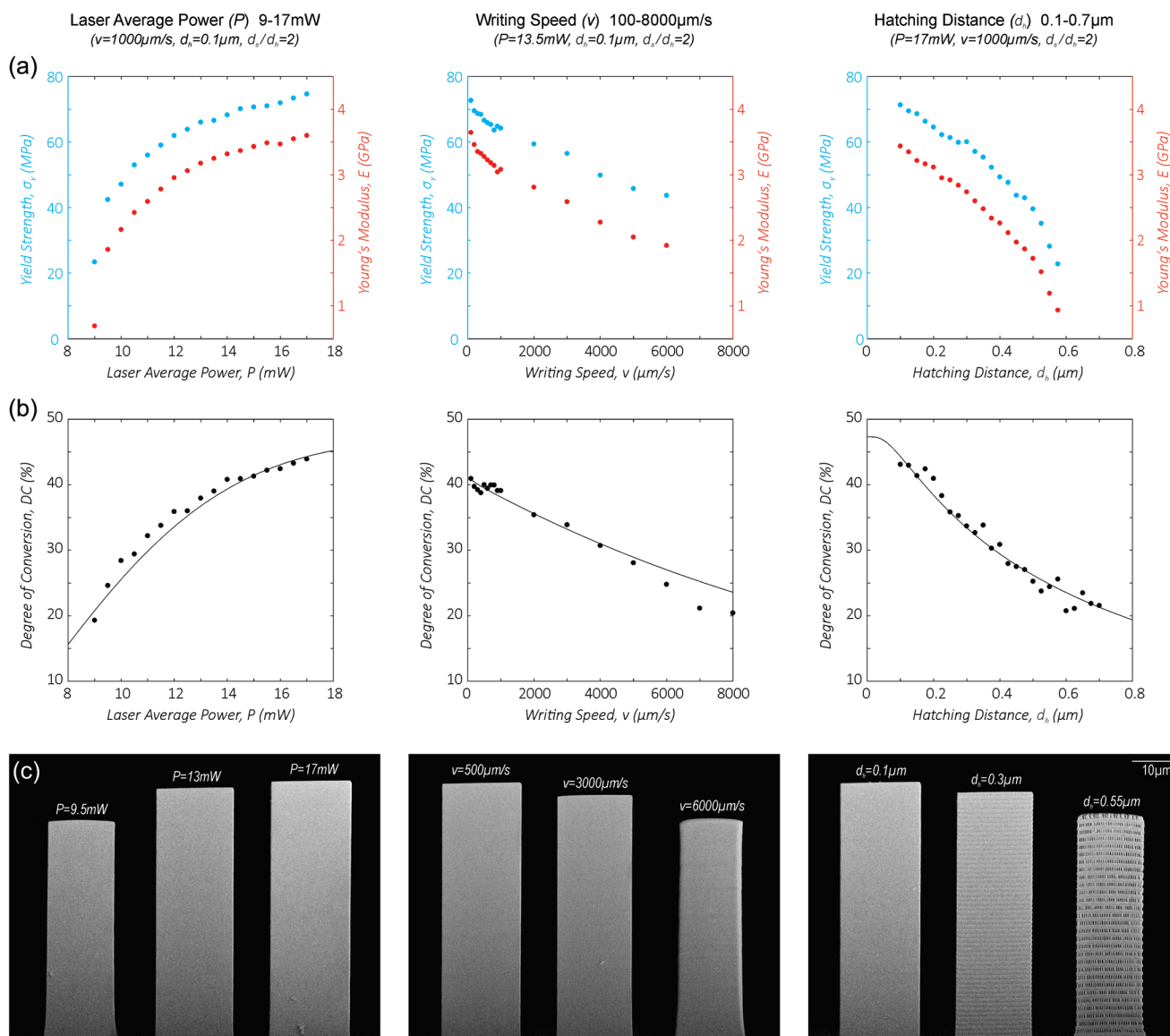
Figure 3. TPP process parameters tailor the mechanical properties of hatched multi-voxel-line specimens. Laser average power (P), writing speed (v) and hatching distance (d_h) (left to right column) have a characteristic impact on a) compressive yield strength (σ_y), Young's modulus (E) and b) degree of conversion (DC). Measured DC values are complemented by analytical predictions (Equation (6)). c) SEM images of selected specimens.

$v > 6000$ µm s^{-1} and $d_h \geq 0.6$ µm, specimen quality starts to significantly degrade, making mechanical tests unfeasible. The found dependencies well translate to other ratios d_s/d_h (Figure S2, Supporting Information), whereby the effective properties slightly shift corresponding to the varying writing density.

Combining all experimental results from Figure 3, shows a linear dependency of E and σ_y with the DC (**Figure 4**). Independent from specific process parameters, specimens with the same DC roughly have the same mechanical properties. E and σ_y approximately increase with the DC as

$$E = (9.52\,DC - 0.56)\,GPa \tag{4}$$

$$\sigma_y = (170.36\,DC - 0.84)\,MPa \tag{5}$$

Conversely, the above equations allow estimation of the DC of individual voxel-lines, which may hardly be measured directly due to their small dimensions. With the average voxel-line strength and stiffness, Equations (4) and (5) estimate a DC of ≈30%.

The tensile properties of hatched multi-voxel-lines specimens well correspond to the compressive properties and their process parameter dependency. Under tension (Figure S3, Supporting Information), increasing P from 9.5 to 17 mW, with $v = 1000$ µm s^{-1}, $d_h = 0.1$ µm and $d_s/d_h = 2$, increases E from 1.5 to 3.5 GPa, the same as under compression (Figure 3). At
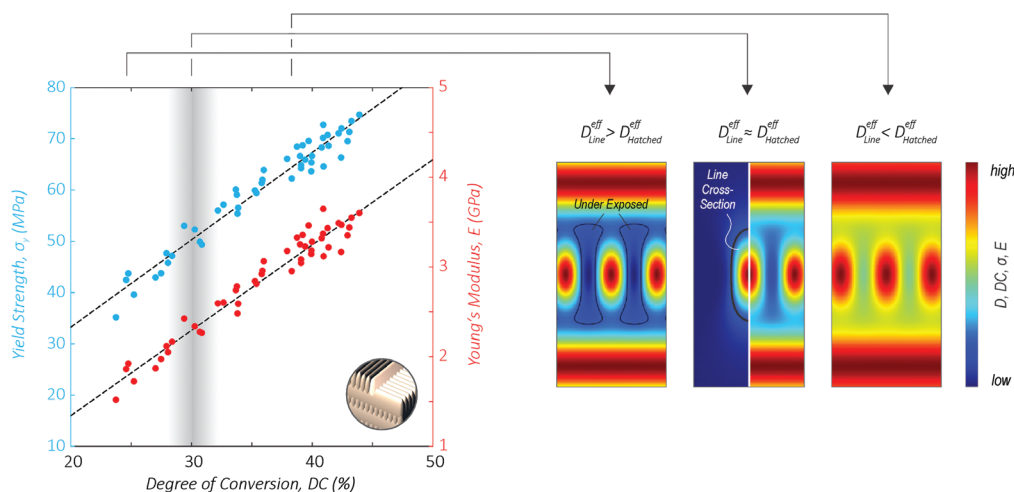
Figure 4. Combining the mechanical property data of hatched specimens from Figure 3 shows linear scaling with the degree of conversion (DC), independent from specific process parameters. With increasing laser average power (P), decreasing writing speed (v) or decreasing hatching distance (d_h) the dose distributions of neighboring exposures increasingly overlap. Depending on the extent of overlap, the "memory effect" creates additional, weaker cross-linked material (effective properties reduced with respect to solitary voxel-lines) or further cross-links previously formed above threshold material (effective properties increased with respect to solitary voxel-lines). Data points of nonporous, fully formed specimens are shown.

the same time, the ultimate tensile strength varies between 115 and 230 MPa.

The measured relations between TPP process parameters and mechanical properties (Figures 3 and 4) are found to be universal for a large range of process parameter combinations. **Figure 5**a shows the dependency of the DC of hatched multi-voxel-line specimens on both P and v over a range of 5–50 mW and 400–100 000 µm s^{-1}, respectively, with d_h = 0.1 µm and d_s/d_h = 2. While trends remain similar, they become milder with increasing v. Over a large field of combinations of P and v, the accessible DC range of roughly 20–45% corresponds to the results of Figures 3 and 4. For v > 50 000 µm s^{-1}, the maximum DC before overexposure starts to drop and is below 35% for v = 100 000 µm s^{-1}.

With increasing dimensions of hatched multi-voxel-line specimens, the mechanical properties decrease. Increasing the edge length of square-shaped compression bars from 2 to 80 µm decreases the DC from 41% to 33%; similarly, E and σ_y decrease from 3 to 2.3 GPa and from 64 to 56 MPa, respectively (Figure S4, Supporting Information). Bulk specimens of 0.4 × 0.4 × 1.2 cm nominal size are cured by single-photon flood exposure. Compressive yield strength and Young's Moduli of up 65 MPa and 3.3 GPa are measured, respectively. In contrast to TPP-derived microbars, the bulk specimens are affected by spalling and hairline cracks, which are present prior to testing (Figure S5, Supporting Information). We measure the density of bulk specimens as 1.25 ± 0.01 g cm^{-3}, which is about 6% higher than the density of the liquid resin.[53]
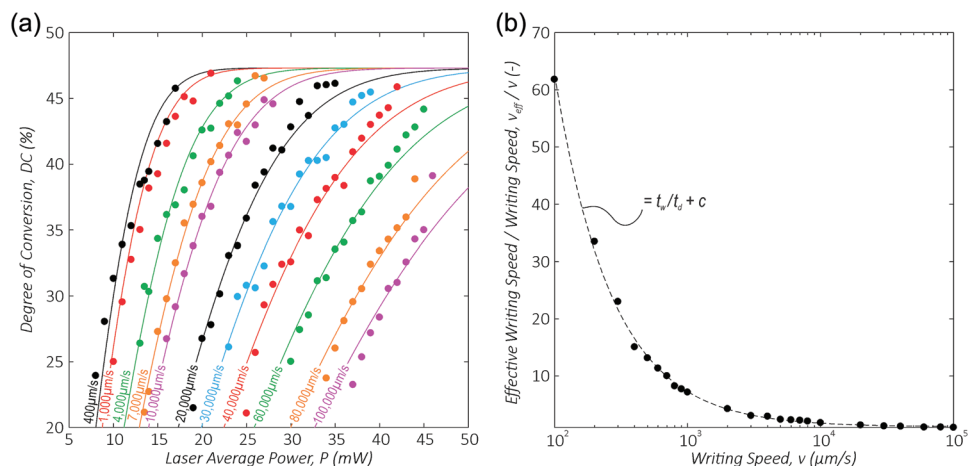

Figure 5. A threshold-based model predicts the degree of conversion (DC) depending on the TPP process parameters. a) Experimental data and predictions (Equation (6)) for a range of combinations of laser average power (P) and writing speed (v). b) With the effective writing speed (v_{eff}) the predictive model accounts for diffusion afflicted polymerization; values of v_{eff}/v determined based on all conducted experiments (Figures 3 and 5a) are proportional to the ratio of writing to diffusion time (t_w/t_d).

3. Discussion

3.1. Single Voxel-Line Specimens

Knowledge of the mechanical properties of individual TPP features is key for a thorough understanding of the mechanisms determining the mechanical behavior of TPP-derived parts. However, difficulties in reliable fabrication of nanoscale specimens, in combination with strain measurement challenges (due to charging of the polymer inside the SEM) and low stiffness and strength of the material (resulting in very small loads) make mechanical experiments challenging. The limited number of existing studies are based on indirect, error-prone measurements, reporting the nanomechanical behavior of TPP materials to be subjected to pronounced size effects, with properties orders of magnitudes lower than bulk counterparts.[30,54,55] By providing the first direct measurement of the mechanical properties of individual TPP features, our study in contrast shows good agreement with typical bulk values of IP-Dip and other common TPP polymers,[56–59] and the absence of pronounced size effects.

The dynamic range of TPP resins is thought to be limited by the solubility and the damage threshold; however, our observed size and process parameter insensitivity of the mechanical properties of voxel-lines may suggest the presence of a third, mobility threshold (m) (Figure 2d). Above a mobility threshold radical density (ρ_m), steric hindrance may inhibit polymerization, "trapping" active species in the already solidified polymer and thus preventing further cross-linking.[60,61] Ideally, the mechanical properties of two-photon polymerized voxel-lines may be assumed to gradually decrease from the inside to the outside, correlating with the spatial laser beam profile.[48] As the process parameters are varied, the corresponding exposure dose distribution shifts relative to the polymerization threshold, changing both the size of the voxel-line and the effective value of the above-threshold portion of the exposure dose distribution in the voxel-line volume. Assuming the mechanical properties proportional to ρ, and solving Equation (2) for the cross-sectional plane of a solitary voxel-line (see the Experimental Section), gives a pronounced process parameter dependency of the effective mechanical properties ($m = \infty$). Figure 2d shows the spatial distributions and effective values of ρ. Without a mobility threshold, one may expect a pronounced increase of the effective ρ across the range of laser average powers applied to form voxel-line specimens printed with $v = 10$ µm s^{-1}. Although this trend may not transfer exactly to the degree of conversion and the mechanical properties, it nonetheless disagrees with the found plateau in E and σ_y (Figure 2c). By contrast, assuming that polymerization is limited by ρ_m cuts the maximum mechanical properties in the voxel-line core corresponding to $\rho = \rho_m$. Depending on the ratio of m/th this yields a much milder dependency of the effective properties on the process parameters (Figure 2d), which correlates well with our experimental data. As ρ_m approaches ρ_{th}, property gradients in the voxel-line cross-section disappear, whereby $\rho_m = \rho_{th}$ itself may not be reached as it implies ideal threshold behavior. Our experimental data (Figure 2c) suggest $m \approx 3$th. With $m = 3$ and DC$^{eff} \approx 30\%$, Figure 2d estimates DC$_{th} \approx 14\%$ and DC$_m \approx 42\%$, which is in good agreement with the accessible DC range measured for multi voxel-line specimens.

3.2. Hatched Multi-Voxel-Line Specimens

The pronounced tailorability of the mechanical properties of hatched two-photon-polymerized material compared to solitary voxel-lines may primarily be caused by the "memory effect." Depending on the combination of P, v, d_h, and d_s, the dose distributions of neighboring exposures overlap to different extents. Simply speaking, neighboring voxel-lines increasingly overlap as they become "larger" (with increasing P and decreasing v) and as d_h and d_s are reduced, thus creating a bandwidth of effective properties even if those of corresponding solitary voxel-lines would be identical. Thereby, existing insoluble material with relatively low DC, like the surface region of previously solitary voxel-lines, is further cross-linked, producing an increase in the effective properties relative to those of solitary voxel-lines. Conversely, "smaller" constituent voxel-lines (produced by decreasing P and increasing v) and larger d_h and d_s limit overlap to the below-threshold Gaussian wings of neighboring exposures, thus introducing less cross-linked material between constituent voxel-lines and reducing the effective properties of hatched structures. Examples of property distributions with lower, equivalent and higher effective values than individual voxel-lines are qualitatively sketched in Figure 4. For d_h and d_s above the resolution limit, below-threshold Gaussian tails can be dissolved during development, yielding a porous material as shown in Figure 3c. Hatched specimens with a DC of ≈30% have the same strength and stiffness as solitary voxel-lines, suggesting that formation of less cross-linked material and further cross-linking of previously formed above-threshold material cancel each other out, yielding a composite hatched material that is on average mechanically equivalent to a single line.

In contrast to solitary voxel-lines, the impact of a mobility threshold on multi-voxel-line materials is uncertain. With the mobility threshold, the maximum effective properties of a hatched material may be reached once the entire material volume approaches DC$_m \approx 42\%$; this well agrees with the maximum DC from Figures 3 and 4. However, the same DC values are also found to approach the damage threshold. Compared to a hatched material, an individual line exposure can have a significantly higher dose before the damage threshold is reached. In a hatched material the damage threshold may be reached before a mobility threshold can have a notable effect. The somewhat lower tensile strength of hatched specimens (loaded perpendicular to printing direction) with respect to voxel-line specimens (loaded parallel to printing direction) (Figure 1c), indicates that hatching, even in a high DC material, may still yield anisotropic composite-like behavior.

To reduce the process time, shell-scaffold printing strategies leave certain enclosed material volumes in the liquid state and cross-link those by single-photon flood-exposure subsequently to TPP.[62] Compared to point-by-point TPP exposure, single-photon flood exposure simultaneously cross-links a large material volume. With increasing part size, this may notably reduce the radical mobility and hence the maximally achievable DC

and mechanical properties. At the same time, we have observed increasing flaw nucleation. Yield strengths and Young's Moduli of the presented, several millimeter-size flood-exposed specimens are 7% and 8% lower than the respective maximum values of TPP-derived specimens. For sufficiently small volumes, the mechanical properties of the enclosed material may be similar to the maximum values obtained via TPP.

With decreasing writing speed, TPP of hatched materials increasingly deviates from the ideal "memory effect"-based model.[45] As the time between the exposures of neighboring lines increases, below-threshold active species of a first exposure diffuse away before the next exposure would increase their concentration to a high enough level to form insoluble material. Typical specimens in this study had an edge length (a) of 20 µm and were printed with $d_h = 0.1$ µm and $d_s = 0.2$ µm. The average time which elapses between the writing of two neighboring lines (t_w) can be approximated as $(a + a^2/d_h)/2v \approx 2000$ µm/v. The critical diffusion path length (d) for an active species not to be affected by a subsequent exposure can be estimated as the distance between neighboring lines plus the TPP resolution (r). With Abbe's diffraction limit providing $r = \lambda/(2\,\text{NA})$,[63] $d \geq 0.6$ µm may be obtained. Fick's second law approximates the diffusion time (t_d) as $t_d \approx 2\delta/d^2$,[64] with the diffusion coefficient (δ). For photoinitiator molecules in liquid solution, δ is on the order of 10^{-1}–10^2 µm^2 s^{-1}.[49,65] These estimates provide a critical writing speed $v_{crit} \approx (a + a^2/d_h)\delta/d^2 \approx 10^3$–$10^5$ µm s^{-1}. Below v_{crit}, diffusion reduces the DC with respect to an ideal, diffusion-free polymerization. Writing speeds in this study range from 10^1–10^5 µm s^{-1}, indicating that the measured properties are diffusion affected at the lower writing speeds.

A simple threshold-based model predicts the experimentally measured dependencies of the mechanical properties on P, v, and d_h. Assuming a linear correlation between ρ and DC, Equations (2) and (3) provide

$$\text{DC} = c_1\,\rho_0\left(1 - e^{-\delta_{2,eff}\,c_0\frac{P^2}{v_{eff}}D_V}\right) + c_2 \tag{6}$$

with the constant (c_0) comprising the relevant optical parameters of the TPP process (see the Experimental Section) and the proportionality constants (c_1) and (c_2). To account for molecular diffusion, the actual writing speed (v) is replaced by an effective writing speed (v_{eff}).[66] Other effects, such as temperature-dependent diffusion are not accounted for but may need to be considered for higher laser pulse widths than used here.[67] Nonlinear least square fitting of all presented DC data provides the explicit dependency of v_{eff} on v (Figure 5b), and gives $c_1\rho_0 = 0.62$, $c_2 = -0.15$, and $D_V = c_3/d_h^n$ with $c_3 = 1.5e4$ µm$^{-2.36}$ and $n = 0.64$. With v replaced by v_{eff}, the presented TPP model well predicts diffusion-affected polymerization (Figures 3b and 5a), whereas it would drastically overestimate properties with the actual writing speed (v) instead.[28] Combining Equation (6) with Equations (4) and (5) provides the relationships between strength and stiffness and the process parameters. This allows to individually program a large range of mechanical properties of TPP-derived parts by simple process parameter adjustment.

Whereas the effective writing speed has been introduced as a simple fudge factor,[66] our data shows that it may be derived from molecular diffusion physics. The ratio v_{eff}/v is proportional to t_w/t_d and, for a diffusion coefficient of 0.55 µm^2 s^{-1}, can be closely approximated by $v_{eff}/v = t_w/t_d + c$, with $c = 1.13$ (Figure 5b). For low writing speeds, v_{eff} substantially exceeds v, while in the 10^4 µm s^{-1} range the difference between v_{eff} and v drops below 10%. Notice that $v_{eff} \rightarrow v$ as the writing speed increases (e.g., as $t_w/t_d \rightarrow 0$), supporting the argument that molecular diffusion becomes negligible at high writing speeds. At the same time though, those high writing speeds seem to increase the local heat influx, potentially causing the decrease of the damage threshold that we observe (Figure 5a), which lowers the achievable maximum mechanical properties.

The above diffusion considerations are consistent with the measured size-dependence on the mechanical properties of hatched pillars (Figure S4, Supporting Information). The critical writing speed below which diffusion needs to be considered is proportional to the part size. For a given writing speed, parts become increasingly diffusion affected as their dimensions increase, resulting in a decrease of their mechanical properties. Similarly, the toolpath can be expected to have an influence. To maximize the mechanical properties, optimized toolpath strategies could reduce the average time in between the exposure of neighboring lines, e.g., by consecutive instead of parallel printing of individual features, by breaking large features down into several smaller ones, or by decreased writing density of volumes without high surface finish requirements (Figure S6, Supporting Information).

The observed dependencies may be expected to transfer to different resin systems, processing conditions, and printing strategies, however, it is emphasized that specific quantitative relations may differ. A full understanding of all polymerization-relevant processes, and their dependency on printing patterns, part geometry, and resin chemistry will require further in-depth experimental characterization and combined photonics- and molecular dynamics-based modeling. The model presented in this work is an approximation based on a paraxial Gaussian light intensity distribution. While this condition is not rigorously justified at the high numerical apertures used here, it is sufficient as i) the highest intensity part of the light distribution at the focal point can be described by a Gaussian envelope, and ii) the laser pulse width encompasses many optical cycles.[46,52,68] If desired, higher degree of precision could be achieved by a photonics model based on Debye vectorial diffraction theory.[69,70] Beyond the printing parameters, other process conditions, such as the details of the development strategy, may also affect some properties of TPP-derived materials and would need to be considered.[32]

4. Conclusion

This study provides insight into the mechanical behavior of two-photon-polymerized individual voxel-line features and derives the mechanisms controlling the effective properties of parts which are hatched from multiple voxel-lines. We systematically show that the mechnical properties, precision and process time of the acrylate-based resin IP-Dip can be vastly tailored via corresponding TPP process parameter selection. With a threshold-based model we accurately predict the

**ADVANCED
SCIENCE NEWS**

www.advancedsciencenews.com

**ADVANCED
MATERIALS
TECHNOLOGIES**

www.advmattechnol.de

processing-structure-properties relation, laying the foundation for a universal quantitative predictability of the mechanical properties of TPP-derived materials.

The characterization methodology presented herein may serve as general framework to establish a standardized knowledge base for TPP material systems. In future studies, the dependencies found herein may thereby enable substantial reduction of experimental characterization. Our findings may be expected to transfer to different acrylate-based and other resins systems, and provide meaningful knowledge for ongoing effort to overcome major technological challenges of TPP, including increasing the resolution,[63,71] and developing novel printable materials.[72–74] In particular, this study may help to understand and optimize the properties of TPP-derived ceramics and metals.[74,75] The demonstrated broad bandwidth of properties furthermore opens up vistas for novel concepts of pseudo-multi-material design with locally tailorable properties and optimized response to complex external loads.

5. Experimental Section

Fabrication: All specimens were manufactured from the photoresist Ip-Dip (Nanoscribe GmbH). TPP was performed using a Photonic Professional GT (Nanoscribe GmbH) DLW system equipped with a Plan-Apochromat 63 × 1.4 Oil DIC M27 (Carl Zeiss AG) objective and a FemtoFiber pro NIR (TOPTICA Photonics AG) laser, with a center wave length (λ) of 780 nm, a pulse width (τ) of ≈100 fs, and a repetition rate (f) of 80 MHz.[76] The laser average power value (P) is the mean power value at the aperture of the objective, with 100% corresponding to 50 mW.[76] A transmittance of the objective (T) of 65% was measured.

Specimens were printed on fused silica substrates in a layer-by-layer sequence using the system's galvanometric mirror scanning mode. After DLW, samples were submerged in propylene glycol monomethyl ether acetate (PGMEA) for 20 min, to dissolve uncured photoresist, followed by a 5 min long isopropanol bath for further cleaning. Subsequently, specimens were dried using an Autosamdri-931 (Tousimis Research Corp. Inc.) critical point dryer operated in the auto mode. To minimize effects of varying process conditions on the measured properties, the experimental routines were precisely kept consistent and were carried out in a climate-controlled environment.

Voxel-line specimens were manufactured as dumbbell-shaped compression and tensile bars with gauge sections consisting of one individual voxel-line of uniform elliptical cross section. Widths and heights of the gauge sections of 190–640 nm and 670–1850 nm, respectively, were realized by different combinations of P and the writing speed (v). The dumbbell-shape of compression bars was chosen to increase the contact area between the test bar and the measurement system. Gauge sections of compression bars had slenderness ratios of 11 to 15:1.[77] Hatched multi-voxel-line specimens were manufactured in a [0/90] laminate manner from unidirectional layers with a hatching distance (d_h) between the axes of neighboring voxel-lines and a slicing distance (d_s) between neighboring layers. Compression bars were designed as uniform square-shaped bars with a height-to-edge length ratio of 3.25 and nominal edge lengths of 2–80 µm. Tensile specimens were designed as push-to-pull mechanisms.[78] The gauge section of dumbbell-shaped tensile bars had a uniform rectangular shape of 4 × 3.2 × 9.5 µm. Bulk samples of 4 × 4 × 12 mm nominal size were cured for 60 min via single-photon flood exposure, using a LQ-Box (Rolence Enterprise Inc.) UV-lamp with a peak wavelength of 405 nm and an average light intensity of 150 mW cm^{-2}.

Experimental Characterization: Specimen dimensions were optically measured using a FEI Magellan 400XHR (Thermo Fisher Scientific Inc.) SEM. To determine E, σ_y, and σ_{UTS}, uniaxial compression and tension experiments were performed at a constant strain rate of 0.001 s^{-1}. Voxel-line experiments were carried out with a FT-NMT03 (FemtoTools AG) nanomechanical testing system equipped with a FT-S200 sensor. Focused ion beam (FIB) milling was used to cut tensile grippers into the FT-S200 sensor in a FEI Quanta 3D FEG (Thermo Fisher Scientific Inc.) dual beam (SEM/FIB). For multi-voxel-line specimens an Alemnis Nanoindenter (Alemnis AG) equipped with a flat punch diamond tips, 400 µm in diameter, was used. Bulk specimens were compressed with the Universal testing frame Instron 8800 (Instron, ITW Inc.). Load–displacement curves were recorded. For the voxel-line and multi-voxel-line tensile specimens, the displacement was corrected for equipment and substrate compliances via a digital image correlation (DIC) algorithm developed in house. Applying the measured dimensions, engineering stress and strain were determined. E was extracted as the maximum slope of the linear elastic regime and σ_y as the 0.2% yield offset of the corresponding stress–strain curve.[77,79] σ_{UTS} was the maximum engineering tensile stress at specimen rupture. The density of bulk specimens was determined with the nominal dimensions and the weight, measured with a M-prove scale (Sartorius AG).

Raman spectroscopy was used to determine the DC of multi-voxel line compression specimens. Raman spectra were acquired using an inVia (Renishaw plc) confocal Raman microscope with a 50× objective, operated at an excitation wavelength of 785 nm, with a laser intensity of 50% and an exposure time of 1.5–2 s averaged over 15 acquisitions. DC values were extrapolated from Raman spectra as

$$DC = 1 - \left(\frac{A_{C=C}/A_{C=O}}{A'_{C=C}/A'_{C=O}} \right) \tag{7}$$

with the integrated intensities of carbon–carbon and carbon–oxygen double bond peaks $A_{C=C}$ and $A_{C=O}$ in the polymerized resin, and $A'_{C=C}$ and $A'_{C=O}$ the integrated intensities of the same peaks in the unpolymerized resin.[28] $A_{C=C}$ and $A_{C=O}$ were determined by fitting Lorentzian and Voigt functions to the respective peaks.

Analytical Model: The photon flux intensity distribution (I) during exposure in the cross-sectional plane of an infinite voxel-line in a Cartesian system, with its length along the x-axis, is the superposition of a train of femtosecond laser pulses, scanned in x-direction with v. For the writing speeds used here the transit time across an observation point is much longer than the duration of a laser pulse and the photon flux intensity is effectively static. Assuming a Gaussian laser beam, $I(x, y, z, t)$, where the y–z plane corresponds to the voxel-line cross-section, can be written as[47,51]

$$I(x, y, z, t) = I_0 \left(\frac{w_0^2}{w(z)^2} \right) e^{\frac{-2\left((x+vt)^2 + y^2\right)}{w(z)^2}} \tag{8}$$

with the peak photon flux intensity (I_0), the beam radius ($w(z)$) along the propagation direction (z) and the beam waist ($w_0 = w(0)$). vt accounts for the position of the center of the beam at the time (t). The beam radius is defined as $w(z) = w_0 \sqrt{1 + (z/z_R)^2}$ with the Rayleigh length ($z_R = (\pi w_0^2)/\lambda$) and the excitation wavelength (λ). w_0 can be approximated by the radius of the central airy disk (0.61 λ/NA),[52,68] with the numerical aperture of the focusing optics (NA).

Evaluation of Equation (1) with Equation (8), at an observation plane $x = 0$ which the beam passes at $t = 0$ gives

$$\int_0^\rho \frac{d\rho}{(\rho_0 - \rho)} = \delta_{2,\text{eff}} \, I_0^2 \left(\frac{w_0^4}{w(z)^4} \right) \int_{-\infty}^\infty e^{\frac{-4\left((vt)^2 + y^2\right)}{w(z)^2}} \, dt \tag{9}$$

which after integration yields the radical density distribution $\rho(y, z)$ in the cross-sectional plane of the voxel-line

$$\rho(y, z) = \rho_0 \left(1 - \exp\left[-\delta_{2,\text{eff}} I_0^2 \left(\frac{w_0^4}{w(z)^3} \right) \sqrt{\frac{\pi}{4}} \frac{f\tau}{v} e^{\frac{-4y^2}{w(z)^2}} \right] \right) \tag{10}$$

**ADVANCED
SCIENCE NEWS**

www.advancedsciencenews.com

**ADVANCED
MATERIALS
TECHNOLOGIES**

www.advmattechnol.de

with the laser repetition rate (f), and the pulse width (τ). I_0 can be expressed in terms of the laser average power (P) as

$$I_0 = \frac{2e^2}{e^2-1}\left(\frac{TP\lambda}{\pi w_0^2 \tau fhc}\right) \tag{11}$$

with the fraction of light transmitted through the magnification optics (T), Planck's constant (h) and the speed of light in vacuum (c).[80,81] With Equation (11), the effective radical density in the voxel-line cross-section can be expressed in terms of P and ν as

$$\rho = \rho_0\left(1-\exp\left[-\delta_{2,\text{eff}}c_0\frac{P^2}{\nu}D_V\right]\right) \tag{12}$$

where (c_0) comprises the optical parameters and numerical factors and with the mean value of the term $\exp((-4y^2)/(w(z)^2))/w(z)^3$ over the voxel-line cross-section (D_V). Equation (12) is also valid for a hatched material with ideal memory effect behavior, however, D_V may only be determined numerically. $\delta_{2,\text{eff}}$ has been taken as 3×10^{-55} cm^{4}s.[46] Although a constant τ was used, it is noted that $\delta_{2,\text{eff}}$ and therefore the radical density are sensitive to the pulse width.[67] Voxel-line dimensions are given by $\rho(y, z) = \rho_{\text{th}}$, nonlinear least square fitting of the measured voxel-line dimensions with Equation (10) gave a ratio of ρ_{th} to ρ_0 of 0.0793, which agrees with reported values of other TPP photoresists.[46]

Supporting Information

Supporting Information is available from the Wiley Online Library or from the author.

Conflict of Interest

The authors declare no conflict of interest.

[1] T. Baldacchini, *Three-Dimensional Microfabrication Using Two-Photon Polymerization*, Elsevier, Amsterdam **2015**.

[2] K.-S. Lee, R. H. Kim, D.-Y. Yang, S. H. Park, *Prog. Polym. Sci.* **2008**, *33*, 631.

[3] J. K. Hohmann, M. Renner, E. H. Waller, G. von Freymann, *Adv. Opt. Mater.* **2015**, *3*, 1488.

[4] C. M. Soukoulis, M. Wegener, *Nat. Photonics* **2011**, *5*, 523.

[5] G. von Freymann, A. Ledermann, M. Thiel, I. Staude, S. Essig, K. Busch, M. Wegener, *Adv. Funct. Mater.* **2010**, *20*, 1038.

[6] J. Bauer, L. R. Meza, T. A. Schaedler, R. Schwaiger, X. Zheng, L. Valdevit, *Adv. Mater.* **2017**, *29*, 1701850.

[7] D. Martella, S. Nocentini, D. Nuzhdin, C. Parmeggiani, D. S. Wiersma, *Adv. Mater.* **2017**, *29*, 1704047.

[8] H. Zeng, D. Martella, P. Wasylczyk, G. Cerretti, J.-C. G. Lavocat, C.-H. Ho, C. Parmeggiani, D. S. Wiersma, *Adv. Mater.* **2014**, *26*, 2319.

[9] T.-Y. Huang, M. S. Sakar, A. Mao, A. J. Petruska, F. Qiu, X.-B. Chen, S. Kennedy, D. Mooney, B. J. Nelson, *Adv. Mater.* **2015**, *27*, 6644.

[10] H. Zeng, P. Wasylczyk, C. Parmeggiani, D. Martella, M. Burresi, D. S. Wiersma, *Adv. Mater.* **2015**, *27*, 3883.

[11] S. Tottori, L. Zhang, F. Qiu, K. K. Krawczyk, A. Franco-Obregón, B. J. Nelson, *Adv. Mater.* **2012**, *24*, 811.

[12] A. Marino, O. Tricinci, M. Battaglini, C. Filippeschi, V. Mattoli, E. Sinibaldi, G. Ciofani, *Small* **2018**, *14*, 1702959.

[13] F. Klein, B. Richter, T. Striebel, C. M. Franz, G. Von Freymann, M. Wegener, M. Bastmeyer, *Adv. Mater.* **2011**, *23*, 1341.

[14] A. Marino, C. Filippeschi, G. G. Genchi, V. Mattoli, B. Mazzolai, G. Ciofani, *Acta Biomater.* **2014**, *10*, 4304.

[15] O. Tricinci, T. Terencio, B. Mazzolai, N. M. Pugno, F. Greco, V. Mattoli, *ACS Appl. Mater. Interfaces* **2015**, *7*, 25560.

[16] M. Röhrig, M. Thiel, M. Worgull, H. Hölscher, *Small* **2012**, *8*, 3009.

[17] B.-K. Hsiung, R. H. Siddique, L. Jiang, Y. Liu, Y. Lu, M. D. Shawkey, T. A. Blackledge, *Adv. Opt. Mater.* **2017**, *5*, 1600599.

[18] G. Nelson, R. A. Kirian, U. Weierstall, N. A. Zatsepin, T. Faragó, T. Baumbach, F. Wilde, F. B. P. Niesler, B. Zimmer, I. Ishigami, M. Hikita, S. Bajt, S.-R. Yeh, D. L. Rousseau, H. N. Chapman, J. C. H. Spence, M. Heymann, *Opt. Express* **2016**, *24*, 11515.

[19] R. Di Giacomo, S. Krödel, B. Maresca, P. Benzoni, R. Rusconi, R. Stocker, C. Daraio, *Sci. Rep.* **2017**, *7*, 45897.

[20] C. A. Lissandrello, W. F. Gillis, J. Shen, B. W. Pearre, F. Vitale, M. Pasquali, B. J. Holinski, D. J. Chew, A. E. White, T. J. Gardner, *J. Neural Eng.* **2017**, *14*, 036006.

[21] C. Yang, Q. Cao, P. Puthongkham, S. T. Lee, M. Ganesana, N. V. Lavrik, B. J. Venton, *Angew. Chem., Int. Ed.* **2018**, *57*, 14255.

[22] Z. F. Rad, R. E. Nordon, C. J. Anthony, L. Bilston, P. D. Prewett, J.-Y. Arns, C. H. Arns, L. Zhang, G. J. Davies, *Microsyst. Nanoeng.* **2017**, *3*, 17034.

[23] T. Gissibl, S. Thiele, A. Herkommer, H. Giessen, *Nat. Photonics* **2016**, *10*, 554.

[24] Z. Xie, S. Feng, P. Wang, L. Zhang, X. Ren, L. Cui, T. Zhai, J. Chen, Y. Wang, X. Wang, W. Sun, J. Ye, P. Han, P. J. Klar, Y. Zhang, *Adv. Opt. Mater.* **2015**, *3*, 1232.

[25] M. Malinauskas, A. Žukauskas, V. Purlys, K. Belazaras, A. Momot, D. Paipulas, R. Gadonas, A. Piskarskas, H. Gilbergs, A. Gaidukevičiūtė, I. Sakellari, M. Farsari, S. Juodkazis, *J. Opt.* **2010**, *12*, 124010.

[26] N. Lindenmann, G. Balthasar, D. Hillerkuss, R. Schmogrow, M. Jordan, J. Leuthold, W. Freude, C. Koos, *Opt. Express* **2011**, *18*, 1290.

[27] M. Schumann, T. Bückmann, N. Gruhler, M. Wegener, W. Pernice, *Light: Sci. Appl.* **2014**, *3*, e175.

[28] L. J. Jiang, Y. S. Zhou, W. Xiong, Y. Gao, X. Huang, L. Jiang, T. Baldacchini, J.-F. Silvain, Y. F. Lu, *Opt. Lett.* **2014**, *39*, 3034.

**ADVANCED
SCIENCE NEWS**
www.advancedsciencenews.com

**ADVANCED
MATERIALS
TECHNOLOGIES**
www.advmattechnol.de

[29] Z. Bayindir, Y. Sun, M. J. Naughton, C. N. LaFratta, T. Baldacchini, J. T. Fourkas, J. Stewart, B. E. A. Saleh, M. C. Teich, *Appl. Phys. Lett.* **2005**, *86*, 064105.

[30] S. Nakanishi, S. Shoji, S. Kawata, H.-B. Sun, *Appl. Phys. Lett.* **2007**, *91*, 063112.

[31] E. D. Lemma, F. Rizzi, T. Dattoma, B. Spagnolo, L. Sileo, A. Qualtieri, M. De Vittorio, F. Pisanello, *IEEE Trans. Nanotechnol.* **2016**, 1.

[32] J. S. Oakdale, J. Ye, W. L. Smith, J. Biener, *Opt. Express* **2016**, *24*, 27077.

[33] D. Bourell, J. P. Kruth, M. Leu, G. Levy, D. Rosen, A. M. Beese, A. Clare, *CIRP Ann.* **2017**, *66*, 659.

[34] D. Herzog, V. Seyda, E. Wycisk, C. Emmelmann, *Acta Mater.* **2016**, *117*, 371.

[35] W. J. Sames, F. A. List, S. Pannala, R. R. Dehoff, S. S. Babu, *Int. Mater. Rev.* **2016**, *61*, 315.

[36] W. E. King, A. T. Anderson, R. M. Ferencz, N. E. Hodge, C. Kamath, S. A. Khairallah, A. M. Rubenchik, *Appl. Phys. Rev.* **2015**, *2*, 041304.

[37] L. H. Nguyen, M. Straub, M. Gu, *Adv. Funct. Mater.* **2005**, *15*, 209.

[38] T. Baldacchini, C. N. Lafratta, R. A. Farrer, M. C. Teich, B. E. A. Saleh, M. J. Naughton, J. T. Fourkas, *J. Appl. Phys.* **2004**, *95*, 6072, .

[39] C. Decker, *Acta Polym.* **1994**, *45*, 333.

[40] W. H. Teh, U. Dürig, U. Drechsler, C. G. Smith, H.-J. Güntherodt, *J. Appl. Phys.* **2005**, *97*, 054907.

[41] J. Torgersen, X.-H. Qin, Z. Li, A. Ovsianikov, R. Liska, J. Stampfl, *Adv. Funct. Mater.* **2013**, *23*, 4542.

[42] A. Ovsianikov, J. Viertl, B. Chichkov, M. Oubaha, B. Maccraith, I. Sakellari, A. Giakoumaki, D. Gray, M. Vamvakaki, M. Farsari, C. Fotakis, *ACS Nano* **2008**, *2*, 2257.

[43] B. Kaehr, N. Ertas, R. Nielson, R. Allen, R. T. Hill, M. Plenert, J. B. Shear, *Proc. Natl. Acad. Sci. U.S.A.* **2006**, *78*, 3198.

[44] C. A. Coenjarts, C. K. Ober, *Chem. Mater.* **2004**, *16*, 5556.

[45] E. Waller, G. von Freymann, E. H. Waller, G. von Freymann, *Polymers* **2016**, *8*, 297.

[46] J. Serbin, A. Egbert, A. Ostendorf, B. N. Chichkov, R. Houbertz, G. Domann, J. Schulz, C. Cronauer, L. Fröhlich, M. Popall, *Opt. Lett.* **2003**, *28*, 301.

[47] S. Shukla, X. Vidal, E. P. Furlani, M. T. Swihart, K.-T. Kim, Y.-K. Yoon, A. Urbas, P. N. Prasad, *ACS Nano* **2011**, *5*, 1947.

[48] J. T. Fourkas, in *Three-Dimensional Microfabrication Using Two-Photon Polymerization* (Ed: T. Baldacchini), William Andrew Publishing, New York, NY **2016**, pp. 45–61.

[49] A. Pikulin, N. Bityurin, *Phys. Rev. B* **2007**, *75*, 195430.

[50] T. Bormann, B. Müller, M. Schinhammer, A. Kessler, P. Thalmann, M. de Wild, *Mater. Charact.* **2014**, *94*, 189.

[51] H. E. Williams, C. Diaz, G. Padilla, F. E. Hernandez, S. M. Kuebler, *J. Appl. Phys.* **2017**, *121*, 223104.

[52] G. De Miguel, G. Vicidomini, B. Harke, A. Diaspro, in *Three-Dimensional Microfabrication Using Two-Photon Polymerization* (Ed: T. Baldacchini), Elsevier, New York, NY **2016**, pp. 190–220.

[53] Nanoscribe GmbH, *Safety Data Sheet: IP-Dip Photoresist*, **2013**.

[54] S. Ushiba, K. Masui, N. Taguchi, T. Hamano, S. Kawata, S. Shoji, *Sci. Rep.* **2015**, *5*, 17152.

[55] H.-B. Sun, K. Takada, S. Kawata, *Appl. Phys. Lett.* **2001**, *79*, 3173.

[56] R. Feng, R. J. Farris, *J. Micromech. Microeng.* **2003**, *13*, 80.

[57] J. Stampfl, S. Baudis, C. Heller, R. Liska, A. Neumeister, R. Kling, A. Ostendorf, M. Spitzbart, *J. Micromech. Microeng.* **2008**, *18*, 125014.

[58] K. Terzaki, M. Kissamitaki, A. Skarmoutsou, C. Fotakis, C. A. Charitidis, M. Farsari, M. Vamvakaki, M. Chatzinikolaidou, *J. Biomed. Mater. Res., Part A* **2013**, *101A*, 2283.

[59] M. Liu, J. Sun, Y. Sun, C. Bock, Q. Chen, *J. Micromech. Microeng.* **2009**, *19*, 035028.

[60] C. Decker, K. Moussa, *J. Polym. Sci., Part A: Polym. Chem.* **1987**, *25*, 739.

[61] M. Wen, A. V. Mccormick, *Macromolecules* **2000**, *33*, 9247.

[62] X. Zhou, Y. Hou, J. Lin, *AIP Adv.* **2015**, *5*, 030701.

[63] J. Fischer, M. Wegener, *Opt. Mater. Express* **2011**, *1*, 614.

[64] D. A. Porter, K. E. Easterling, M. Y. Sherif, *Phase Transformations in Metals and Alloys*, CRC Press Taylor & Francis Group, Boca Raton **2009**.

[65] N. Fang, C. Sun, X. Zhang, *Appl. Phys. A* **2004**, *79*, 1839.

[66] M. G. Guney, G. K. Fedder, *J. Micromech. Microeng.* **2016**, *26*, 105011.

[67] B. Tan, K. Venkatakrishnan, A. Makaronets, *Des. Monomers Polym.* **2013**, *16*, 145.

[68] K. Khuen Seet, S. Juodkazis, V. Jarutis, H. Misawa, *Appl. Phys. Lett.* **2006**, *89*, 024106.

[69] M. Gu, *Advanced Optical Imaging Theory*, Springer, Berlin **2000**.

[70] T. Kondo, K. Yamasaki, S. Juodkazis, S. Matsuo, V. Mizeikis, H. Misawa, *Thin Solid Films* **2004**, *453–454*, 550.

[71] P. Mueller, M. Thiel, M. Wegener, *Opt. Lett.* **2014**, *39*, 6847.

[72] Z. C. Eckel, C. Zhou, J. H. Martin, A. J. Jacobsen, W. B. Carter, T. A. Schaedler, *Science.* **2016**, *351*, 58.

[73] F. Kotz, K. Arnold, W. Bauer, D. Schild, N. Keller, K. Sachsenheimer, T. M. Nargang, C. Richter, D. Helmer, B. E. Rapp, *Nature* **2017**, *544*, 337.

[74] A. Vyatskikh, S. Delalande, A. Kudo, X. Zhang, C. M. Portela, J. R. Greer, *Nat. Commun.* **2018**, *9*, 593.

[75] J. Bauer, A. Schroer, R. Schwaiger, O. Kraft, *Nat. Mater.* **2016**, *15*, 438.

[76] Nanoscribe GmbH, *Photonic Professional (GT) User Maual*, **2017**.

[77] ASTM International, *Standard Test Method for Compressive Properties of Rigid Plastics*, **2008**.

[78] J. Bauer, A. Schroer, R. Schwaiger, I. Tesari, L. Valdevit, O. Kraft, *Extreme Mech. Lett.* **2015**, *3*, 105.

[79] ASTM International, *Standard Test Method for Tensile Properties of Plastics*, **2003**.

[80] X.-Z. Dong, Z.-S. Zhao, X.-M. Duan, *Appl. Phys. Lett.* **2008**, *92*, 091113.

[81] R. Menzel, *Photonics : Linear and Nonlinear Interactions of Laser Light and Matter*, Springer, Berlin **2007**.